RESEARCH ARTICLE OPEN ACCESS

Variations in ECM Topography, Fiber Alignment, Mechanical Stiffness, and Cellular Composition Between Ventral and Dorsal Ligamentum Flavum Layers: Insights Into Hypertrophy Pathogenesis

Ting-Yuan Tu[1,2,3] | Yu-Chia Hsu[4] | Chia-En Yang[1] | Yan-Jye Shyong[5] | Cheng-Hsiang Kuo[3,6] | Yuan-Fu Liu[4] | Shu-Shien Shih[2] | Cheng-Li Lin[2,4,7,8]

[1]Department of Biomedical Engineering, College of Engineering, National Cheng Kung University, Tainan, Taiwan | [2]Medical Device Innovation Center, National Cheng Kung University, Tainan, Taiwan | [3]International Center for Wound Repair and Regeneration, National Cheng Kung University, Tainan, Taiwan | [4]Department of Orthopedic Surgery, National Cheng Kung University Hospital, College of Medicine, National Cheng Kung University, Tainan, Taiwan | [5]Department of Clinical Pharmacy and Pharmaceutical Sciences, National Cheng Kung University, Tainan, Taiwan | [6]Department of Biochemistry and Molecular Biology, College of Medicine, National Cheng Kung University, Tainan, Taiwan | [7]Musculoskeletal Research Center, Innovation Headquarters, National Cheng Kung University, Tainan, Taiwan | [8]Skeleton Materials and Bio-Compatibility Core Lab, Research Center of Clinical Medicine, National Cheng Kung University Hospital, College of Medicine, National Cheng Kung University, Tainan, Taiwan

Correspondence: Cheng-Li Lin (jengli94@gmail.com)

Received: 10 July 2024 | **Revised:** 22 October 2024 | **Accepted:** 3 December 2024

Funding: This work was supported by the National Cheng Kung University Hospital, NCKUH-11302030, NCKUH-11306015, and NCKUH-11310001, National Science and Technology Council, MOST110-2314-B-006-027-MY3, NSTC 112-2314-B-006-075, NSTC 112-2628-B-006-014-MY3, and NSTC 112-2636-B-006-001-MY3.

Keywords: extracellular matrix | ligamentum flavum hypertrophy | mechanical property | myofibroblast

ABSTRACT

Background: Previous studies have suggested that changes in the composition of the extracellular matrix (ECM) play a significant role in the development of ligamentum flavum hypertrophy (LFH) and the histological differences between the ventral and dorsal layers of the hypertrophied ligamentum flavum. Although LFH is associated with increased fibrosis in the dorsal layer, comprehensive research exploring the characteristics of the ECM and its mechanical properties in both regions is limited. Furthermore, the distribution of fibrosis-associated myofibroblasts within LFH remains poorly understood. This study aimed to bridge the existing knowledge gap concerning the intricate relationships between ECM characteristics, mechanical properties, and myofibroblast expression in LFH.

Methods: Histological staining, scanning electron microscopy, and atomic force microscopy were used to analyze the components, alignment, and mechanical properties of the ECM. Immunostaining and western blot analyses were performed to assess the distribution of myofibroblasts in LF tissues.

Results: There were notable differences between the dorsal and ventral layers of the hypertrophic ligamentum flavum. Specifically, the dorsal layer exhibited higher collagen content and disorganized fibrous alignment, resulting in reduced stiffness.

Abbreviations: AFM, atomic force microscopy; CD34, cluster of differentiation 34; ECL, enhanced chemiluminescence; ECM, extracellular matrix; EDTA, ethylenediaminetetraacetic acid; EGFR, epidermal growth factor receptor; ELISA, enzyme-linked immunosorbent assay; EVG, elastin van gieson; H&E, hematoxylin and eosin; IHC, immunohistochemistry; LDH, lumbar disc herniation; LF, ligamentum flavum; LFH, ligamentum flavum hypertrophy; LSS, lumbar spinal stenosis; SEM, scanning electron microscopy; TGF-β, transforming growth factor beta; VEGF, vascular endothelial growth factor; α-SMA, alpha-smooth muscle actin.

Immunohistochemistry analysis revealed a significantly greater presence of α-smooth muscle actin (αSMA)-stained cells, a marker for myofibroblasts, in the dorsal layer.

Conclusions: This study offers comprehensive insights into LFH by elucidating the distinctive ECM characteristics, mechanical properties, and cellular composition disparities between the ventral and dorsal layers. These findings significantly enhance our understanding of the pathogenesis of LFH and may inform future research and therapeutic strategies.

1 | Background

Ligamentum flavum hypertrophy (LFH) is the major contributor of lumbar spinal stenosis (LSS), a degenerative condition that significantly impacts mobility and quality of life [1]. As the ligament thickens, it progressively narrows the spinal canal, compressing neural structures and leading to pain and neurological deficits [2, 3]. This thickening involves not just an increase in tissue mass but profound changes in the composition and architecture of the ligament, including increased collagen deposition and loss of elasticity [4–7]. These structural distortions contribute to the biomechanical dysfunction of the ligament, resulting in spinal canal narrowing [8]. Understanding the biomechanical properties and the factors driving these structural changes is essential for unraveling the pathogenesis of LFH [9, 10].

Extracellular matrix (ECM) remodeling is pivotal in the progression of LFH [6]. In hypertrophied ligamentum flavum (LF) compared to normal specimens from patients with lumbar disc herniation (LDH), serving as the control group, there is a notable increase in collagen deposition and a reduction in elastin fibers, resulting in diminished flexibility and disrupted tissue architecture [5, 11]. These changes, however, are not uniform across the ligament [12, 13]. Previous research has identified more pronounced pathological changes in the dorsal hypertrophied LF, including a higher collagen-to-elastin ratio and disoriented elastin fibers, potentially associated mechanical stress distribution or growth factor activity [5, 6, 13, 14]. While differences between the ventral and dorsal LF layers have been sporadically reported, this region-specific ECM topography highlights the need to investigate both layers in detail, as the fiber alignment and structural changes in each region could have distinct effects on the overall biomechanical functions in the LF [15].

The biomechanical properties of the LF are intricately linked to its mechanical stress, ECM composition, and cellular dynamics [16, 17]. Notably, the dorsal layer experiences higher mechanical stress during spinal movements, particularly in flexion [16]. This stress correlates with increased collagen deposition and disorganized fiber alignment, in contrast to the more preserved structure observed in the ventral layer [18, 19]. Aligned ligament tissue has been shown to exhibit greater stiffness compared to disorganized tissue under uniaxial tension, as demonstrated in animal models [12, 20]. Moreover, myofibroblasts, which play a key role in fibrosis, are more prevalent in the dorsal layer of hypertrophied LF [21, 22]. However, most studies have focused on the genetic expression of alpha-smooth muscle actin (α-SMA), without thoroughly investigating protein levels or comparing these dynamics across healthy, ventral, and dorsal layers [21–24]. The inconsistencies in research findings on the mechanical properties of hypertrophied LF, partly due to differences in measurement techniques and small sample sizes [15], underscore the need for a comprehensive study that evaluates these biomechanical and cellular differences across regions.

Currently, there is a critical gap in understanding the relationship between ECM composition, fiber alignment, mechanical stiffness, and cellular composition in the ventral and dorsal layers of hypertrophied LF. We hypothesize that significant disparities in the collagen-to-elastin ratio, ECM organization, biomechanical properties, and cellular composition exist between these two regions in patients with LSS, which may contribute to the pathogenesis of LF hypertrophy and the progression of spinal stenosis. To explore these differences, we characterized the ECM architecture and mechanical properties of hypertrophied LF using electron microscopy and atomic force microscopy (AFM). Additionally, cellular density, composition, and the distribution of myofibroblast-associated proteins were assessed through immunohistochemistry (IHC) and western blot analysis. This comprehensive approach seeks to bridge the knowledge gap regarding ECM remodeling, cellular dynamics, and mechanical stiffness between the ventral and dorsal regions of hypertrophied LF.

2 | Methods

2.1 | Participants

We recruited patients who had undergone lumbar spine surgery at a tertiary hospital in Taiwan. Before surgery, all patients underwent magnetic resonance imaging (MRI) to assess the thickness of the LF. The LF thickness was independently measured three times by two experienced spine surgeons, and the mean of these measurements was used as the final LF thickness. During surgery, hypertrophied LF specimens were collected from patients diagnosed with LSS, while nonhypertrophied LF specimens were obtained from patients diagnosed with LDH. The LDH group served as a control for nonhypertrophic LF, whereas the LSS group represented the pathological group with LFH. LF specimens were collected en bloc during spinal decompression surgery and detached from their insertion sites following laminectomy. Based on cadaveric studies [1] and surgical observations [6], the LF can be naturally separated into dorsal and ventral parts. This anatomical distinction allowed us to classify the retrieved LF specimens into dorsal and ventral portions. Histological sections were prepared parallel to the long axis of the LF fibers, ensuring optimal visualization of fiber orientation and structural changes.

2.2 | Experimental Design

Specimens were divided into four groups: the LDH group as the control, the LSS group with the whole specimen, and the LSS-ventral and LSS-dorsal groups based on anatomical layers. The ECM pattern was analyzed by calculating the collagen/elastin ratio using hematoxylin and eosin (H&E) and Elastin van Gieson (EVG) staining, quantifying fiber alignment through EVG staining and scanning electron microscopy (SEM), and measuring stiffness using atomic force microscopy (AFM). LF cell density and myofibroblast distribution were determined by IHC staining. The expression of myofibroblast-associated proteins α-SMA was quantified using western blot analysis. Experimental details are provided in Figure 1.

2.3 | Histological Stains

LF specimens were sectioned, fixed, and dehydrated in 30% sucrose-PBS at 4°C for 24 h. Subsequently, tissues were embedded in paraffin, cut into 4-μm thick slices using a paraffin microtome, and after dewaxing, antigen retrieval, and blocking. The sections were incubated overnight at 4°C with primary antibodies, washed, and detected using a DAB kit, followed by hematoxylin counterstaining. H&E staining was used for histology analysis. Some slides were stained using the Elastic Stain Kit (Verhoeff Van Gieson/EVG Stain) (Abcam, USA) according to the manufacturer's protocol. Elastin was identified using a solution of ferric chloride, iodine, and Verhoeff's hematoxylin, while collagenous connective tissue was stained with Van Gieson's solution.

2.4 | Scanning Electron Microscope (SEM)

Fresh LF tissue samples were sectioned, collected, and fixed in 2.5% glutaraldehyde at 4°C overnight. Following fixation, the samples underwent gradual dehydration using an alcohol gradient with immersion in 50% and 75% alcohol for 20 min each, followed by storage in 75% alcohol. Tissue drying was achieved using a Critical Point Dryer (Samdri-PVT-3D, Tousimis, USA) after two consecutive 20-min replacements with 95% alcohol. The dried specimens were carefully placed in microcentrifuge tubes, sealed with paraffin film, and stored in moisture-proof boxes until further testing. For scanning electron microscopy (SEM), samples were affixed to a stage using carbon tape, platinum-plated, and photographed. The SEM evaluation of ultrastructural fiber arrangement was conducted in accordance with the method described by Zhao et al. [11].

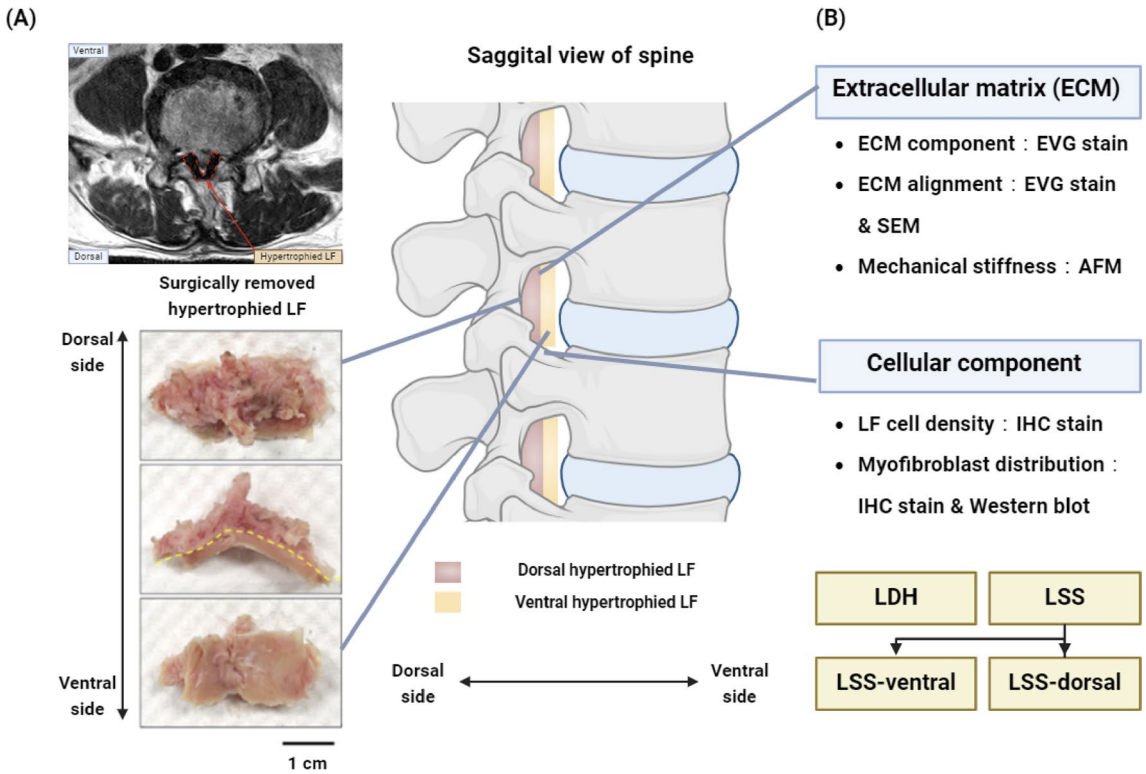

FIGURE 1 | The experimental design of the study. (A) T2-weighted MRI image of hypertrophied LF at the L4/5 level, delineated by the red dotted line. Intraoperative photographs of hypertrophied ligamentum flavum specimens are categorized into ventral and dorsal segments based on their anatomical location. The upper image shows the dorsal LF specimen, the middle image displays the junction between the dorsal and ventral LF (yellow dashed line), and the lower image presents the ventral LF specimen (scale bar: 1 cm). (B) Experimental design of the study. Evaluation of ECM patterns using EVG staining through SEM to assess ECM composition and alignment, and AFM to measure mechanical stiffness. IHC staining was used to determine cell density and evaluate myofibroblasts, while protein expression of α-SMA was quantified using Western blot analysis. The LDH group served as the control, and comparisons were made between the LDH and LSS group, and within the LSS group between ventral and dorsal regions to assess histological differences.

2.5 | Image and Data Analysis

For the evaluation of EVG-stained tissue, ImageJ software was utilized to identify the colors corresponding to elastic and collagen fibers. The areas occupied by these fibers were measured to determine the collagen/elastin ratio. Fiber alignment analysis was conducted using the OrientationJ plugin in ImageJ, which allowed for the exploration of fiber orientation angles and provided coherency measurements indicating the consistency of fiber alignment [25]. A coherency value of 1 indicates a dominant orientation in the local structure, while a value of 0 indicates isotropy in the local neighborhood. Cell density and α-SMA positive cells were detected using QuPath software.

2.6 | Stiffness Measurement

Immediately after specimen retrieval, specimens were soaked in 20% glycerol at 4°C overnight for dehydration. Glycerol was then removed, and specimens were immersed in optimal cutting temperature compound at 4°C overnight to ensure thorough tissue impregnation. Finally, specimens were frozen at −20°C, completing the freeze-embedding process. Frozen blocks were cut into 25-μm thick slices using a Cryostat Microtome (CM1860, LEICA, Germany) and mounted on silane-coated slides. Within 1 week, sections were analyzed using AFM. The selection of AFM and its protocol follows the methodologies outlined by Essmann et al. and Jezek et al., chosen for its proven experimental stability, reliability, and high-resolution force measurement capabilities in assessing the mechanical properties of complex biological tissues [15, 26]. A CSC12/tipless/noAl cantilever (MikroMasch, Wetzlar, Germany) modified with a 25 μm polystyrene bead (in diameter), spring constant ranging from 0.2 to 0.6 N/m and 1 nN indenting force was used. The cantilever approached and retracted at rates of 1 μm/s. Data were processed using JPK package software based on the Hertz model. To compare LDH and LSS tissues, 30 test points were randomly selected across the entire tissue area. Additionally, EVG-stained serial sections aided in region selection, with 30 points measured on both ventral and dorsal sides of LSS tissue to obtain regional results.

2.7 | Western Blot Analysis

LF tissues were lysed using a lysis buffer containing 1% Triton X-100 (Sigma-Aldrich, Taiwan), 50 mM Tris (pH 7.5), 10 mM EDTA, 0.02% NaN_3, and a protease inhibitor mixture (Roche Boehringer Mannheim Diagnostics, Mannheim, Germany). The tissues were homogenized using a PowerMasher II (Nippi, Japan). Total protein concentration was determined using the Bradford method with bovine serum albumin as the standard. After electrophoresis, proteins were transferred onto PVDF membranes (Millipore, Billerica, MA, USA). The membrane was then blocked with 5% nonfat dried milk in PBST for 1 hour at room temperature. Following blocking, the membrane was incubated overnight at 4°C with primary antibodies (α-SMA) (abcam, ab7817) [21]. Subsequently, the PVDF membrane was washed with PBST and incubated with secondary antibody for 1 hour at room temperature. Proteins were visualized using ECL detection kit.

2.8 | Statistical Analysis

Regarding patient characteristics, data are reported as mean ± SD (standard deviation). All histological and cellular experiments were conducted at least three times. Student's *t*-test was used for data analysis, with statistical significance set at $p < 0.05$. Data were analyzed using SPSS software (Version 17).

3 | Results

3.1 | Patients and Sample Measurement

A total of 68 patients were included in the study. Hypertrophied LF specimens were collected from 48 patients diagnosed with LSS, and nonhypertrophied LF specimens were obtained from 20 patients diagnosed with LDH. The mean age of the LDH group was 33 ± 9 years old, while the LSS group had a mean age of 70 ± 13 years. The mean LF thickness in the LDH group was 2.72 ± 0.9 mm, compared to 4.56 ± 0.7 mm in the LSS group.

3.2 | ECM Pattern—SEM Imaging Evaluation and Collagen/Elastin Ratio

After staining the LF specimens with EVG, microscopic images of the LDH, LSS, LSS-ventral, and LSS-dorsal groups were captured. Elastin fibers appeared dark blue, whereas collagen fibers appeared pink. The LSS group exhibited histological changes from the ventral to the dorsal region, showing decreased elastin fibers and increased collagen fibers, necessitating division of the LSS sample into ventral and dorsal parts for precise pathogenesis study (Figure 2A).

SEM images were used to examine the ECM structures in these four groups, revealing distinct differences. In the LDH sample, organized branched elastin fiber bundles arranged in straight alignment were observed. In contrast, the LSS group exhibited collagen fibers that overlapped and displayed wave-like patterns with larger diameters than elastin fibers. The LSS-ventral group displayed aligned and branched elastin fiber bundles, similar to those observed in the LDH group. However, the LSS-dorsal group exhibited highly interwoven and disordered thread-like collagen microstructures (Figure 2B).

The LDH group showed a higher abundance of elastin fibers compared to the LSS group. Further categorization into ventral and dorsal regions revealed that the ventral part resembled the LDH group, with dominant elastin fibers in the ECM. Conversely, the LSS-dorsal group showed increased collagen fibers and reduced elastic fibers. Meanwhile, the LSS group ($N = 4$) had a significantly higher collagen/elastin ratio compared to the LDH group ($N = 3$) (1.02 ± 0.21 vs. 0.37 ± 0.30, $p = 0.0218$). Additionally, the LSS-dorsal group ($N = 3$) had a higher ratio compared to the LSS-ventral group ($N = 3$) (5.50 ± 1.85 vs. 0.23 ± 0.159, $p = 0.0081$), indicating differences in ECM composition between the dorsal and ventral regions (Figure 2C,D).

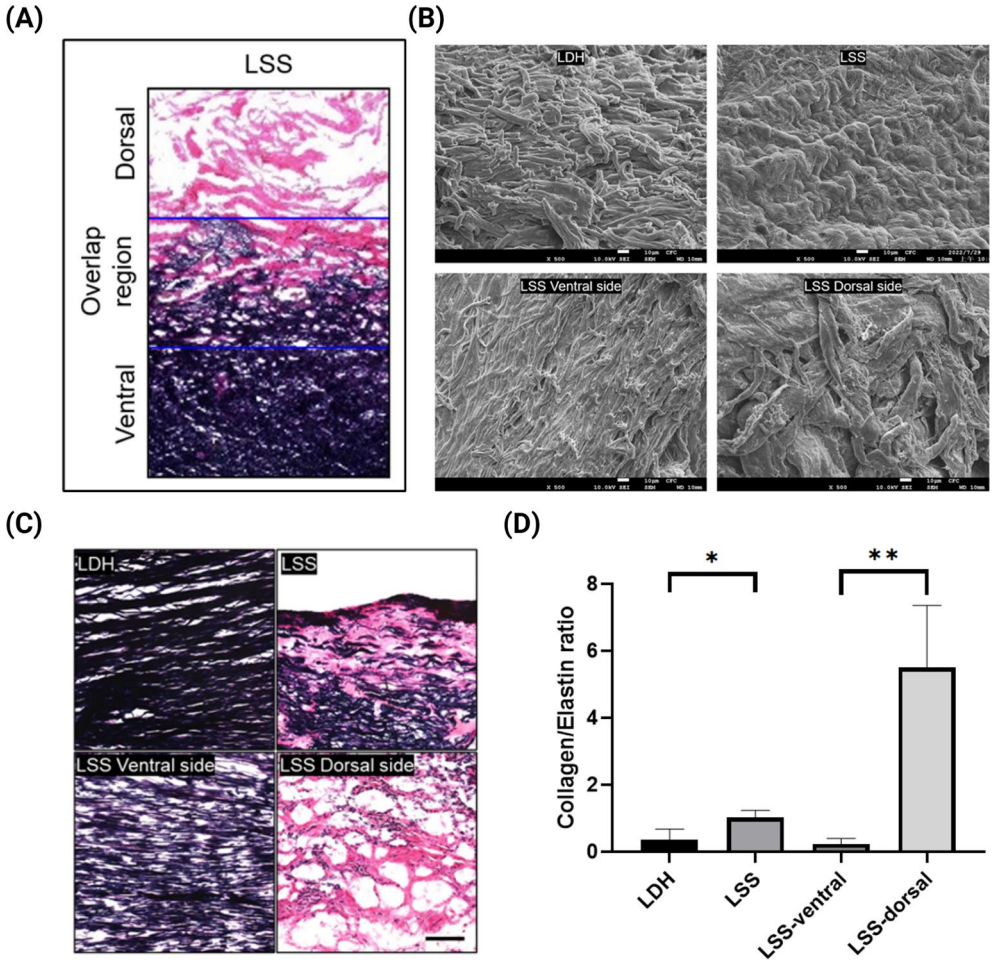

FIGURE 2 | EVG stained sections and collagen/elastin ratio in LDH and LSS groups. (A) Representative images of LSS tissue showing histological transformation from ventral to dorsal regions. (B) SEM images of LF specimens from LDH, LSS, LSS-ventral, and LSS-dorsal groups, highlighting differences in ECM pattern and alignment (scale bar: 10 μm). (C) EVG-stained images of the four groups, with dark blue representing elastin and pink representing collagen. The LDH group showed a higher abundance of elastin fibers compared to the LSS group. The LSS-ventral group exhibited a higher content of elastin fibers than the LSS-dorsal group (scale bar: 50 μm). (D) Quantification analysis of collagen and elastin fiber areas in EVG-stained sections. A collagen/elastin ratio greater than 1 indicates dominance of collagen fibers, and vice versa. All data represent results from above three independent experiments. $^{*}p < 0.05$, $^{**}p < 0.01$.

3.3 | ECM Pattern—Fiber Alignment Coherency

In the histological images of the specimens, yellow dotted lines represented the direction of fiber analysis conducted using image software. The LDH and LSS-ventral groups showed more consistent fiber alignment than the LSS and LSS-dorsal groups (Figure 3A). Fiber alignment data were presented as bar graphs. The LDH and LSS-ventral groups exhibited more concentrated and sharper histograms than the LSS and LSS-dorsal groups, indicating more organized and consistent fiber orientation (Figure 3B). Furthermore, we analyzed alignment direction data using the coherency parameter, which indicates the consistency of fiber alignment. A coherency value of 1 indicates dominant orientation, while a value of 0 indicates isotropic distribution in the local neighborhood. Coherency values were similar between LDH ($N = 12$) and LSS ($N = 33$) groups (0.593 ± 0.172 vs. 0.429 ± 0.228, $p = 0.67$). However, the LSS-dorsal group ($N = 10$) exhibited a significantly lower coherency value than the LSS-ventral group ($N = 12$) (0.257 ± 0.119 vs. 0.690 ± 0.192, $p = 0.03$) (Figure 3C), confirming the disorganized nature of the dorsal region of the hypertrophied LF.

3.4 | Mechanical Property—Stiffness Measured by AFM

AFM was used to measure mechanical stiffness. LF tissue specimens were prepared from the LDH ($N = 3$), LSS ($N = 3$), LSS-ventral ($N = 6$), and LSS-dorsal ($N = 6$) groups, with 30 test points randomly selected across each specimen. Additionally, 10 additional measurements were obtained at evenly spaced 20 mm intervals using a cantilever for both ventral and dorsal LF specimens (Figure 4A).

The bar graph illustrates the average mechanical stiffness values obtained from random measurements in the LDH and LSS groups (Figure 4B). A scatter plot showed the distribution of 30 data points from three patients each in the LDH and

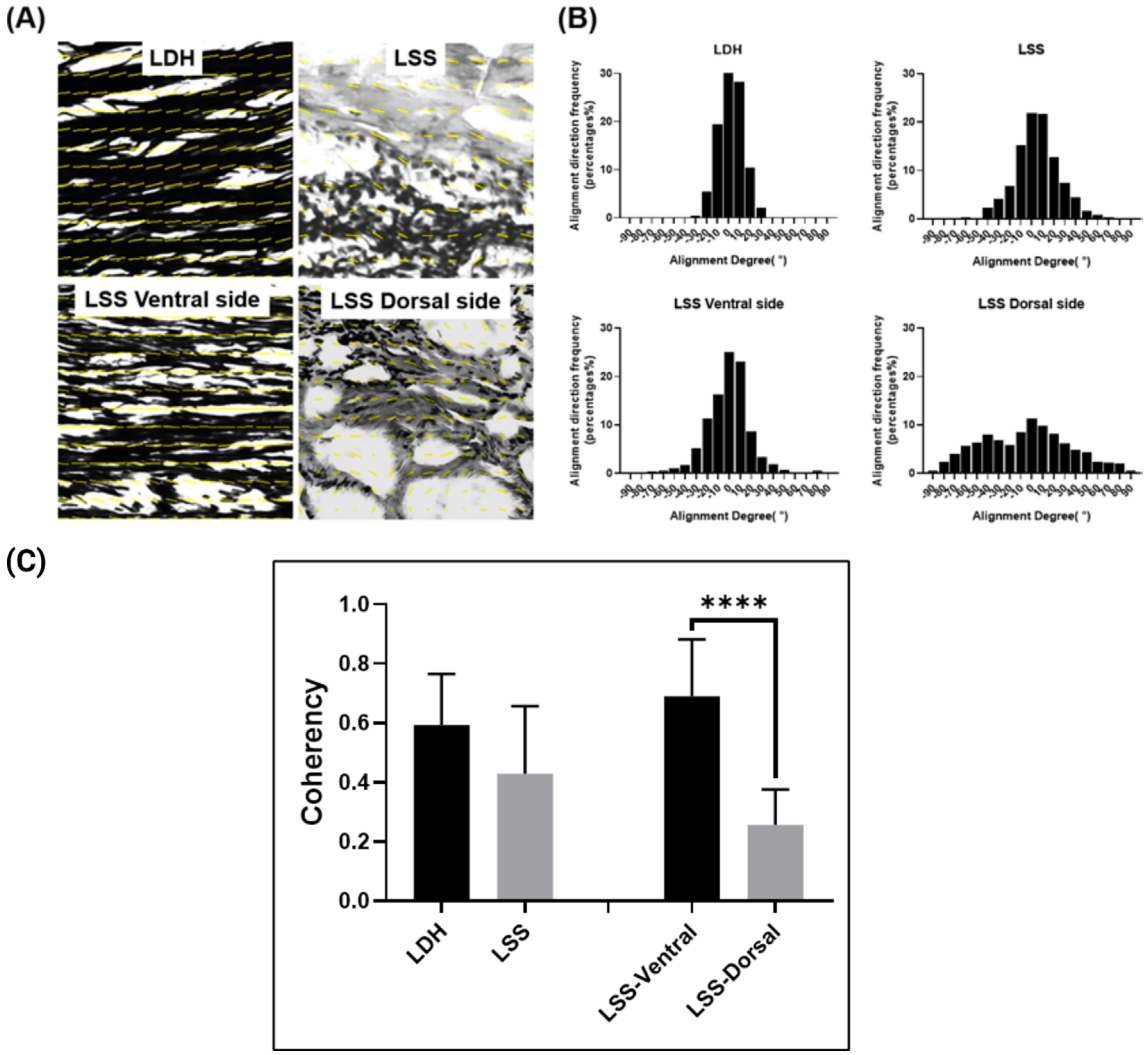

FIGURE 3 | Comparison of fiber alignment coherency in LDH and LSS groups. (A) Representative tissue images show LDH, LSS, LSS-ventral, and LSS-dorsal tissues with alignment direction analysis. Fiber orientation, identified using image software, is indicated by yellow dotted lines. (B) The histogram shows the distribution of fiber alignment directions. (C) Coherency analysis of fiber alignment in four groups. A coherency value of 1 indicates a dominant orientation, while a value of 0 signifies a disorganized fiber direction. All data represent results from three independent experiments. ****$p < 0.0001$.

LSS groups. Results from random measurements indicated a higher mechanical stiffness in the LDH group compared to the LSS group, although the difference did not reach statistical significance (10.58 ± 4.5 vs. 7.11 ± 4.1, $p = 0.38$).

Another bar graph depicted the mean mechanical stiffness values obtained from random measurements in the LSS-ventral and LSS-dorsal groups (Figure 4C). The scatter plot showed data distribution from three patients each in the LSS-ventral and LSS-dorsal specimens. The results revealed that the mechanical property of LSS-ventral was significantly stiffer than LSS-dorsal (18.64 ± 9.0 vs. 3.38 ± 1.8 kPa, $p = 0.002$).

Additionally, the line chart demonstrated different measurement methods and arrayed measurements in LSS-ventral and LSS-dorsal specimens from four patients, indicating significantly lower mechanical stiffness in the LSS-dorsal specimen compared to the LSS-ventral (Figure 4D).

3.5 | LF Tissue—Cell Density

H&E staining was performed on three specimens from LDH, LSS, LSS-ventral, and LSS-dorsal groups. Histological examination revealed higher cell density in the LSS group compared to LDH, with LSS-dorsal specimens showing a more pronounced increase (Figure 5A). Quantitative analysis indicated higher cell density in the LSS group compared to LDH ($N = 3$), though not statistically significant (47.89 ± 8.0 vs. 37.19 ± 1.5, $p = 0.23$). Moreover, cell density in the LSS-dorsal group was significantly higher than LSS-ventral (100.11 ± 24.7 vs. 17.58 ± 2.1, $p = 0.0045$) (Figure 5B). These findings suggest an important role of cell hyperplasia in the pathogenesis of LFH.

3.6 | Myofibroblast Differentiation

Evaluation of myofibroblast differentiation involved examining the distribution of the key marker α-SMA, which indicates

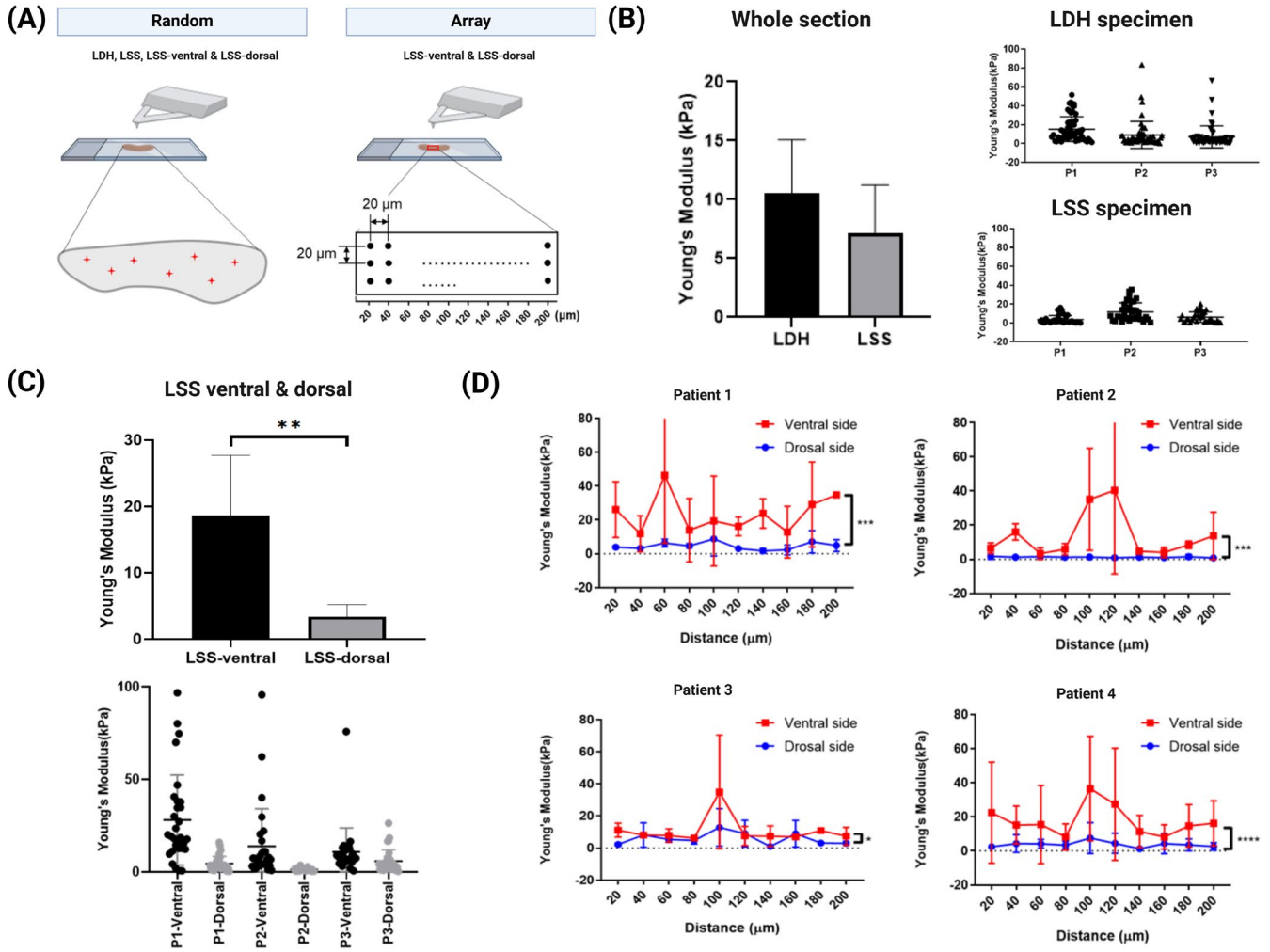

FIGURE 4 | Mechanical stiffness measurement and results analysis. (A) Schematic diagram illustrating two measurement methods. On the left side, 30 random points were tested on each LF specimen from the LDH, LSS, LSS-ventral, and LSS-dorsal group. On the right side, 10 arrayed points with a 20 mm interval were tested on LSS-ventral and LSS-dorsal specimens from four patients. (B) The left bar graph shows the mean values of random measurements for the LDH and LSS groups. The right scatter plot shows the individual data points of random measurements for three patients. (C) The upper bar graph presents the mean values of random measurements for the LSS-ventral and LSS-dorsal groups. The lower scatter plot depicts the individual data points of random measurements for three patients. The mechanical stiffness of the LSS-ventral group was significantly higher than that of the LSS-dorsal group. (D) Individual data points of mechanical stiffness obtained from arrayed measurements in the LSS-ventral and LSS-dorsal groups. In four patients, the mechanical stiffness of the LSS-ventral group was significantly higher than that of the LSS-dorsal group. $^{*}p < 0.05$, $^{**}p < 0.01$, $^{***}p < 0.001$, $^{****}p < 0.0001$.

the presence of myofibroblasts. The results revealed higher expression of α-SMA in the LSS group compared to the LDH group. Additionally, within the LSS group, the LSS-dorsal subgroup showed higher levels of α-SMA expression than the LSS-ventral subgroup (Figure 6A). Quantitative analysis of the IHC staining corroborated these findings, demonstrating similar trends in α-SMA expression between the LSS and LDH groups (57.02 ± 23.5 vs. 43.50 ± 21.9, $p = 0.404$) and between the LSS-ventral and LSS-dorsal groups (86.74 ± 5.5 vs. 37.55 ± 9.9, $p = 0.002$) (Figure 6B). This suggested that myofibroblast differentiation plays a crucial role in ligamentum flavum hypertrophy, particularly in dorsal regions.

Consistent with the IHC staining results, protein expression levels of α-SMA were significantly higher in the LSS group compared to the LDH group ($N = 3$) (0.93 ± 0.1 vs. 0.36 ± 0.2, $p = 0.002$) (Figure 6C). Additionally, there was a significant increase in α-SMA expression levels in the LSS-dorsal group compared to the LSS-ventral group (0.88 ± 0.32 vs. 0.28 ± 0.25, $p = 0.027$) (Figure 6D).

4 | Discussion

The LF plays a crucial role in restricting excessive flexion of the vertebral body and maintaining spinal stability [27]. Its primary constituents include collagen fibers, elastic fibers, reticular fibers, and extracellular matrix, with elastic fibers constituting approximately 80% [18, 28]. However, with advancing age, there is a shift in this composition, leading to an increase in collagen content and a reduction in elasticity, which contribute to LF thickening, and in some cases, calcification and ossification

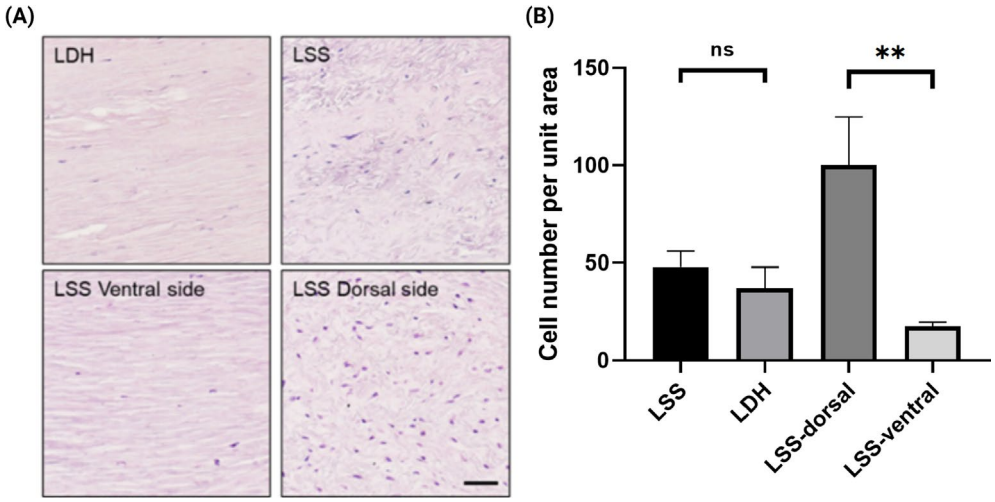

FIGURE 5 | H&E stained specimen and quantitative analysis of cell density. (A) Representative images of LF tissue stained with H&E: Higher cell density was observed in the LSS group compared to the LDH group. The LSS-dorsal group also exhibited higher cell density than the LSS-ventral group. The predominant cell types observed were fibroblasts and inflammatory cells (scale bar: 50 μm) (20× microscope image). (B) Quantitative analysis of cell density: The graph illustrates higher cell density in the LSS group compared to the LDH group. Furthermore, the LSS-dorsal group demonstrated significantly higher cell density compared to the LSS-ventral group. $^{**}p < 0.01$, $n = 3$.

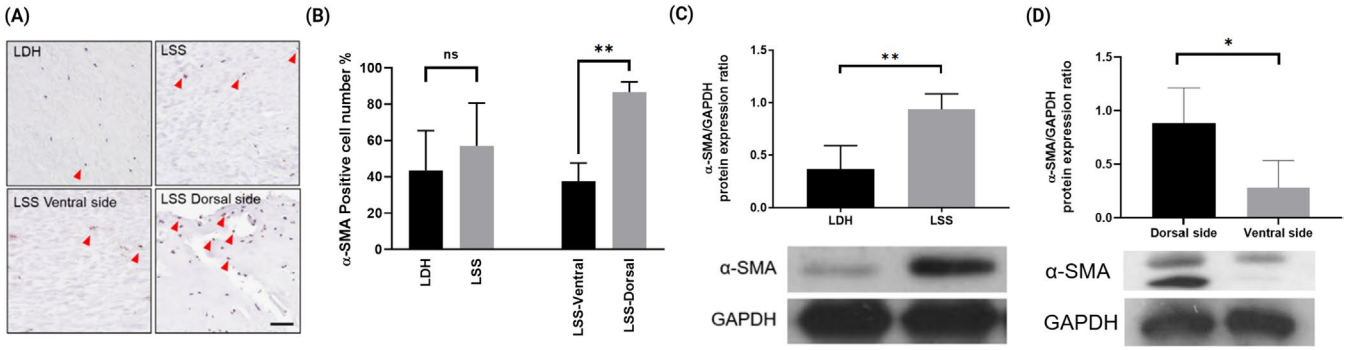

FIGURE 6 | IHC staining and western blot analysis of α-SMA in the LDH, LSS, LSS-ventral, and LSS-dorsal groups. (A) Representative images of LF tissues stained with IHC for α-SMA: Positive staining of cells is indicated by red arrows. (B) Quantification of the percentage of α-SMA-positive cells detected by IHC staining. (C) The LSS group exhibited significantly higher expression of α-SMA compared to the LDH group. (D) α-SMA expression was significantly higher in the LSS-dorsal group compared to the LSS-ventral group. $^{*}p < 0.05$, $^{**}p < 0.01$, $n = 3$.

[5, 6, 29]. This progressive deterioration is further exacerbated by pathological insults, which prompt the LF to undergo hypertrophy as a compensatory response to its weakened mechanical properties [25]. As this hypertrophy progresses, the structural and compositional changes within the LF vary between its dorsal and ventral regions [15]. Understanding these regional differences, particularly the increased collagen-to-elastin ratio and mechanical property shift, is essential for unraveling the pathogenesis of LFH. Therefore, a focused investigation into the differential biomechanical and cellular properties of the dorsal and ventral LF layers is crucial to comprehensively address the mechanical dysfunction associated with LFH.

Given that in most LFH research, histological staining often reveals more dispersed elastin fibers in hypertrophied LF compared to normal specimens from patients with LDH, who serve as the control group [5, 13]. Our study firstly focuses on the compositional and structural differences in the ECM between healthy and hypertrophied LF, particularly highlighting region-specific distinctions between the ventral and dorsal layers. The study demonstrates a significant increase in the collagen/elastin ratio in the dorsal region of the hypertrophied LF, indicating a shift towards a more collagen-rich and less elastic ECM (Figure 2). This finding aligns with observations from a few previous studies, which consistently report an increase in collagen and a decrease in elastin in hypertrophied LF [6, 30]. The disorganization of collagen fiber alignment in the dorsal region, as evidenced by SEM imaging and coherency analysis, adds another layer of complexity to the biomechanical changes in hypertrophied LF. This finding echoes previous studies that have reported the loss of the parallel arrangement of elastic fibers in hypertrophied LF (Figure 3) [13, 19, 31–33].

Distinct mechanical and cellular changes associated with LFH were also observed. While the dorsal region of hypertrophied LF exhibits significant thickening, AFM measurements revealed a notable decrease in mechanical stiffness compared to the ventral region (Figure 4). This paradox may be explained by the increased collagen-to-elastin ratio and disorganized fiber orientation in the dorsal region, which, although contributing to the

overall bulk, compromises its functional integrity [21, 34]. These changes could reflect a compensatory response to repeated microinjuries, where thickening occurs to counteract mechanical weakening [15]. However, at the fibril level as measured by AFM, the tissue remains more prone to injury due to its reduced stiffness and altered structural properties. From a pseudo-macroscopic perspective, the thickened dorsal LF may appear stiffer, but at a finer resolution, its reduced stiffness leaves it vulnerable to further damage. This understanding points to a pathological cycle, where compensatory hypertrophy in response to mechanical stress leads to functional deterioration.

Cell hyperplasia plays a central role in the pathogenesis of LFH, involving key cell types such as fibroblasts, macrophages, endothelial cells, and the recently identified myofibroblasts [21, 22]. In LFH, increased fibroblast and inflammatory cell activity promotes the secretion of fibrotic markers like collagen and vimentin, along with growth factors such as TGF-β1 [15]. Concurrently, fibroblasts are recruited and differentiate into myofibroblasts, driven predominantly by the TGF-β/Smad signaling pathway [35–37]. Myofibroblasts, defined by their contractile properties and increased α-SMA expression, actively contribute to ECM production and tissue remodeling [38]. However, dysregulated myofibroblast apoptosis can lead to excessive fibroproliferation, similar to that seen in other fibrotic conditions, such as hypertrophic scars, renal fibrosis, and cardiac fibrosis [39–41]. A strong association between myofibroblast presence and LFH has been established over the past decade, mirroring findings in other fibroproliferative disorders (Figure 6) [21, 22, 42]. Nevertheless, the exact molecular mechanisms and genetic regulatory pathways governing myofibroblast function in LFH remain poorly understood and require further exploration. Additionally, angiogenesis, as indicated by elevated CD34-positive endothelial cells and VEGF expression, further highlights the complexity of cellular alterations in LFH [4, 43]. Our findings are consistent with these observations, demonstrating pronounced cell hyperplasia in hypertrophied LF, particularly in the dorsal region (Figure 5).

In summary, this study revealed several key insights into LFH. Histological analysis demonstrated increased collagen fiber content, reduced elastic fiber levels, and disorganized fiber orientation in hypertrophied LF. A detailed comparison between the ventral and dorsal regions of hypertrophied LF in LSS patients, as summarized in Table 1, highlights notable differences in tissue composition, structure, mechanical properties, and cellular profiles. We also identified an inverse relationship between the collagen-to-elastin ratio and mechanical stiffness, alongside a positive correlation between ECM alignment and stiffness. These ECM alterations critically influence the biomechanical properties of LF in LSS. The resulting mechanical weakness may predispose the LF to further injury and fibrosis, creating a self-perpetuating cycle of degeneration, as noted in previous studies [15]. In summary, these findings suggest that alterations in collagen and elastic fibers, increased cell density, and the presence of myofibroblasts are likely to contribute to the pathogenesis of LFH.

While this study provides valuable insights into the mechanical and cellular changes associated with LFH, several limitations should be acknowledged. First, in evaluating LF mechanical stiffness, we employed AFM, a novel approach not previously utilized in similar studies, resulting in a lack of comparative data on absolute elastic modulus levels. Second, our study focused on increased expression of myofibroblast-associated markers in hypertrophied LF specimens without exploring genetic regulation, post-transcriptional modifications, or secreted proteomes involved in myofibroblast molecular mechanisms. Future investigations utilizing single-cell sequencing or ELISA could provide valuable insights into these mechanisms in LFH. Third, while we identified elevated collagen content in hypertrophied LF, we did not specify the types of collagen present. Different collagen types may contribute to the diverse molecular mechanisms underlying LFH. Lastly, individual variability in spinal canal diameter may have influenced histological findings due to varying disease severity. Although our methodology followed established protocols and utilized adequate specimen numbers, individual anatomical differences should be considered in interpreting the results [16].

TABLE 1 | Summary of results.

	LSS ventral side	LSS dorsal side
Collagen/elastin ratio	0.237 ± 0.159	5.502 ± 1.856
ECM alignment	0.690 ± 0.192	0.257 ± 0.119
Mechanical stiffness (kPa)	18.64 ± 9.0	3.38 ± 1.8
Cell density (per unit area)	17.58 ± 2.1	100.11 ± 24.7
α-SMA expression	0.28 ± 0.25	0.88 ± 0.32

Note: This table summarizes the key findings of the study, comparing the ventral and dorsal sides of LSS in terms of the collagen/elastin ratio, extracellular matrix (ECM) alignment, mechanical stiffness, cell density, and cell composition.

5 | Conclusion

This study comprehensively investigated the ECM compositions, collagen fiber alignment, mechanical stiffness, and cellular composition in healthy and hypertrophic LF. We found that hypertrophied LF has a higher collagen/elastin fiber ratio and disorganized collagen fiber alignment, leading to decreased mechanical stiffness. Additionally, our study highlights a positive association between myofibroblasts and LFH. These findings enhance our understanding of LFH pathogenesis and suggest potential therapeutic interventions targeting these mechanisms. Future studies should focus on the molecular mechanisms underlying myofibroblast involvement in LFH and explore therapeutic strategies to preserve elastic fibers and improve mechanical properties.

Author Contributions

The authors contributed to this study as follows: Conceptualization: C.L.L., T.Y.T., Y.C.H., and C.E.Y.; Methodology: C.E.Y., Y.J.S., and C.H.K.; Validation: Y.J.S., C.H.K., Y.F.L., and S.S.S.; Formal analysis: C.E.Y.; Investigation: T.Y.T. and S.S.S.; Data curation: C.E.Y. and Y.C.H.; Writing – original draft preparation: Y.C.H. and C.E.Y.; Writing – review and editing: Y.C.H. and C.E.Y.; Visualization: Y.C.H. and C.E.Y.; Supervision: T.Y.T., Y.J.S., C.H.K., and C.L.L.; Project

administration: T.Y.T., Y.J.S., C.H.K., Y.F.L., and C.L.L.; Funding acquisition: C.L.L. All authors have read and approved the final version of the manuscript.

Acknowledgments

The authors would like to express our gratitude to the Skeleton Materials and Bio-Compatibility Core Lab, Research Center of Clinical Medicine, National Cheng Kung University Hospital for their support in conducting this study. The authors are grateful for the support from the Core Research Laboratory, College of Medicine, National Cheng Kung University. The authors also thank the service provided by the Bioimaging Core Facility of the National Core Facility for Biopharmaceuticals, National Science and Technology Council, Taiwan.

Ethics Statement

The study was conducted in accordance with the Declaration of Helsinki and approved by the Institutional Review Board of the National Cheng Kung University Hospital (A-ER-110-001).

Consent

The authors have nothing to report.

Conflicts of Interest

The authors declare no conflicts of interest.

Data Availability Statement

The data used in this study are available from the corresponding author upon request.

References

1. S. D. Trigg and Z. Devilbiss, "Spine Conditions: Lumbar Spinal Stenosis," *FP Essentials* 461 (2017): 21–25.

2. R. K. Jensen, T. S. Jensen, B. Koes, and J. Hartvigsen, "Prevalence of Lumbar Spinal Stenosis in General and Clinical Populations: A Systematic Review and Meta-Analysis," *European Spine Journal* 29, no. 9 (2020): 2143–2163.

3. J. Kim, W. K. Kwon, H. Cho, et al., "Ligamentum Flavum Hypertrophy Significantly Contributes to the Severity of Neurogenic Intermittent Claudication in Patients With Lumbar Spinal Canal Stenosis," *Medicine (Baltimore)* 101, no. 36 (2022): e30171.

4. J. W. Hur, B. J. Kim, J. H. Park, et al., "The Mechanism of Ligamentum Flavum Hypertrophy: Introducing Angiogenesis as a Critical Link That Couples Mechanical Stress and Hypertrophy," *Neurosurgery* 77, no. 2 (2015): 274–281, discussion 281–282.

5. M. Jain, M. Sable, A. P. Tirpude, R. N. Sahu, S. K. Samanta, and G. das, "Histological Difference in Ligament Flavum Between Degenerative Lumbar Canal Stenosis and Non-Stenotic Group: A Prospective, Comparative Study," *World Journal of Orthopedics* 13, no. 9 (2022): 791–801.

6. C. Sun, H. Zhang, X. Wang, and X. Liu, "Ligamentum Flavum Fibrosis and Hypertrophy: Molecular Pathways, Cellular Mechanisms, and Future Directions," *FASEB Journal* 34, no. 8 (2020): 9854–9868.

7. C. L. Lin, Y. T. Kuo, C. H. Tsao, Y. J. Shyong, S. H. Shih, and T. Y. Tu, "Development of an In Vitro 3D Model for Investigating Ligamentum Flavum Hypertrophy," *Biological Procedures Online* 22 (2020): 20.

8. T. Ushiki, "Collagen Fibers, Reticular Fibers and Elastic Fibers. A Comprehensive Understanding From a Morphological Viewpoint," *Archives of Histology and Cytology* 65, no. 2 (2002): 109–126.

9. C.-S. Kim, H. Kim, S. Kim, et al., "Prevalence of and Factors Associated With Stenotic Thoracic Ligamentum Flavum Hypertrophy," *Regional Anesthesia and Pain Medicine* 49, no. 5 (2024): 326–331.

10. S. Diwan, D. Sayed, T. R. Deer, A. Salomons, and K. Liang, "An Algorithmic Approach to Treating Lumbar Spinal Stenosis: An Evidenced-Based Approach," *Pain Medicine* 20, no. Suppl 2 (2019): S23–s31.

11. I. Altun and K. Z. Yüksel, "Histopathological Analysis of Ligamentum Flavum in Lumbar Spinal Stenosis and Disc Herniation," *Asian Spine Journal* 11, no. 1 (2017): 71–74.

12. C. J. Stender, E. Rust, P. T. Martin, E. E. Neumann, R. J. Brown, and T. J. Lujan, "Modeling the Effect of Collagen Fibril Alignment on Ligament Mechanical Behavior," *Biomechanics and Modeling in Mechanobiology* 17, no. 2 (2018): 543–557.

13. P. K. Schräder, D. Grob, B. A. Rahn, et al., "Histology of the Ligamentum Flavum in Patients With Degenerative Lumbar Spinal Stenosis," *European Spine Journal* 8, no. 4 (1999): 323–328.

14. H.-C. Chuang, K. L. Tsai, K. J. Tsai, et al., "Oxidative Stress Mediates Age-Related Hypertrophy of Ligamentum Flavum by Inducing Inflammation, Fibrosis, and Apoptosis Through Activating Akt and MAPK Pathways," *Aging (Albany NY)* 12, no. 23 (2020): 24168–24183.

15. J. Jezek, J. Sepitka, M. Daniel, et al., "The Role of Vascularization on Changes in Ligamentum Flavum Mechanical Properties and Development of Hypertrophy in Patients With Lumbar Spinal Stenosis," *Spine Journal* 20, no. 7 (2020): 1125–1133.

16. Y. X. Peng, Z. Y. Zheng, W. G. Wang, MD, et al., "Relationship Between the Location of Ligamentum Flavum Hypertrophy and Its Stress in Finite Element Analysis," *Orthopaedic Surgery* 12, no. 3 (2020): 974–982.

17. Y. T. Yang, S. J. Zhu, M. L. Xu, et al., "The Biomechanical Effect of Different Types of Ossification of the Ligamentum Flavum on the Spinal Cord During Cervical Dynamic Activities," *Medical Engineering and Physics* 121 (2023): 104062.

18. E. M. Abdel-Meguid, "An Anatomical Study of the Human Lumbar Ligamentum Flavum," *Neurosciences (Riyadh)* 13, no. 1 (2008): 11–16.

19. A. Reyes-Sánchez, C. L. García-Ramos, C. M. Deras-Barrientos, A. Alpizar-Aguirre, L. M. Rosales-Olivarez, and R. Pichardo-Bahena, "Ligamentum Flavum in Lumbar Spinal Stenosis, Disc Herniation and Degenerative Spondylolisthesis. An Histopathological Description," *Acta Ortopédica Mexicana* 33, no. 5 (2019): 308–313.

20. B. K. Connizzo, P. R. Bhatt, K. W. Liechty, and L. J. Soslowsky, "Diabetes Alters Mechanical Properties and Collagen Fiber Re-Alignment in Multiple Mouse Tendons," *Annals of Biomedical Engineering* 42, no. 9 (2014): 1880–1888.

21. F. Hayashi, M. Morimoto, K. Higashino, et al., "Myofibroblasts Are Increased in the Dorsal Layer of the Hypertrophic Ligamentum Flavum in Lumbar Spinal Canal Stenosis," *Spine Journal* 22, no. 4 (2022): 697–704.

22. J. W. Hur, T. Bae, S. Ye, et al., "Myofibroblast in the Ligamentum Flavum Hypertrophic Activity," *European Spine Journal* 26, no. 8 (2017): 2021–2030.

23. S. Ye, W. K. Kwon, T. Bae, et al., "CCN5 Reduces Ligamentum Flavum Hypertrophy by Modulating the TGF-β Pathway," *Journal of Orthopaedic Research* 37, no. 12 (2019): 2634–2644.

24. Y. C. Hsu, H. C. Chuang, K. L. Tsai, et al., "Administration of N-Acetylcysteine to Regress the Fibrogenic and Proinflammatory Effects of Oxidative Stress in Hypertrophic Ligamentum Flavum Cells," *Oxidative Medicine and Cellular Longevity* 2022 (2022): 1380353.

25. K. G. Burt, D. C. Viola, L. E. Lisiewski, J. M. Lombardi, L. F. Amorosa, and N. O. Chahine, "An In Vivo Model of Ligamentum Flavum Hypertrophy From Early-Stage Inflammation to Fibrosis," *JOR Spine* 6, no. 3 (2023): e1260.

26. C. L. Essmann, D. Martinez-Martinez, R. Pryor, et al., "Mechanical Properties Measured by Atomic Force Microscopy Define Health Biomarkers in Ageing *Caenorhabiditis elegans*," *Nature Communications* 11, no. 1 (2020): 1043.

27. J. Li and J. Zhong, "The Hypertrophy of the Cervical Ligamentum Flavum Results in Incomplete Paralysis of Both Lower Limbs: A Case Report," *International Journal of Surgery Case Reports* 113 (2023): 109079.

28. K. Zhang, W. Sun, X. Y. Liu, et al., "Hypertrophy and Fibrosis of the Ligamentum Flavum in Lumbar Spinal Stenosis Is Associated With Increased Expression of LPA and LPAR1," *Clinical Spine Surgery* 30, no. 3 (2017): E189–e191.

29. K. Sairyo, A. Biyani, V. Goel, et al., "Pathomechanism of Ligamentum Flavum Hypertrophy: A Multidisciplinary Investigation Based on Clinical, Biomechanical, Histologic, and Biologic Assessments," *Spine* 30, no. 23 (2005): 2649–2656.

30. Y. Yabe, Y. Hagiwara, A. Ando, et al., "Chondrogenic and Fibrotic Process in the Ligamentum Flavum of Patients With Lumbar Spinal Canal Stenosis," *Spine (Phila Pa 1976)* 40, no. 7 (2015): 429–435.

31. H. Kosaka, K. Sairyo, A. Biyani, et al., "Pathomechanism of Loss of Elasticity and Hypertrophy of Lumbar Ligamentum Flavum in Elderly Patients With Lumbar Spinal Canal Stenosis," *Spine (Phila Pa 1976)* 32, no. 25 (2007): 2805–2811.

32. M. Löhr, J. A. Hampl, J. Y. Lee, R. I. Ernestus, M. Deckert, and W. Stenzel, "Hypertrophy of the Lumbar Ligamentum Flavum Is Associated With Inflammation-Related TGF-β Expression," *Acta Neurochirurgica* 153, no. 1 (2011): 134–141.

33. T. Okuda, I. Baba, Y. Fujimoto, et al., "The Pathology of Ligamentum Flavum in Degenerative Lumbar Disease," *Spine (Phila Pa 1976)* 29, no. 15 (2004): 1689–1697.

34. D. Viejo-Fuertes, D. Liguoro, J. Rivel, D. Midy, and J. Guerin, "Morphologic and Histologic Study of the Ligamentum Flavum in the Thoraco-Lumbar Region," *Surgical and Radiologic Anatomy* 20, no. 3 (1998): 171–176.

35. A. C. Midgley, M. Rogers, M. B. Hallett, et al., "Transforming Growth Factor-β1 (TGF-β1)-Stimulated Fibroblast to Myofibroblast Differentiation Is Mediated by Hyaluronan (HA)-Facilitated Epidermal Growth Factor Receptor (EGFR) and CD44 Co-Localization in Lipid Rafts," *Journal of Biological Chemistry* 288, no. 21 (2013): 14824–14838.

36. X. M. Meng, D. J. Nikolic-Paterson, and H. Y. Lan, "TGF-β: The Master Regulator of Fibrosis," *Nature Reviews. Nephrology* 12, no. 6 (2016): 325–338.

37. J. J. Tomasek, G. Gabbiani, B. Hinz, C. Chaponnier, and R. A. Brown, "Myofibroblasts and Mechano-Regulation of Connective Tissue Remodelling," *Nature Reviews. Molecular Cell Biology* 3, no. 5 (2002): 349–363.

38. B. S. Bagalad, K. M. Kumar, and H. Puneeth, "Myofibroblasts: Master of Disguise," *Journal of Oral and Maxillofacial Pathology: JOMFP* 21, no. 3 (2017): 462–463.

39. G. Gabbiani, "The Myofibroblast in Wound Healing and Fibrocontractive Diseases," *Journal of Pathology* 200, no. 4 (2003): 500–503.

40. S. Meran and R. Steadman, "Fibroblasts and Myofibroblasts in Renal Fibrosis," *International Journal of Experimental Pathology* 92, no. 3 (2011): 158–167.

41. M. Liu, B. L. de Juan Abad, and K. Cheng, "Cardiac Fibrosis: Myofibroblast-Mediated Pathological Regulation and Drug Delivery Strategies," *Advanced Drug Delivery Reviews* 173 (2021): 504–519.

42. A. G. Condorelli, M. el Hachem, G. Zambruno, A. Nystrom, E. Candi, and D. Castiglia, "Notch-Ing Up Knowledge on Molecular Mechanisms of Skin Fibrosis: Focus on the Multifaceted Notch Signalling Pathway," *Journal of Biomedical Science* 28, no. 1 (2021): 36.

43. Y. Matsumoto, T. Fujiwara, R. Imamura, et al., "Hematoma of the Ligamentum Flavum in the Thoracic Spine: Report of Two Cases and Possible Role of the Transforming Growth Factor Beta-Vascular Endothelial Growth Factor Signaling Axis in Its Pathogenesis," *Journal of Orthopaedic Science* 18, no. 2 (2013): 347–354.